

Cite this article as: Pan Lifang, Zhao Kaidong, Wang Shaohua, et al. Plan View Pattern Evolution Rules of Metal Plates During Angular Rolling[J]. Rare Metal Materials and Engineering, 2023, 52(12): 4047-4054. DOI: 10.12442/j.issn.1002-185X.20230300.

ARTICLE

Plan View Pattern Evolution Rules of Metal Plates During Angular Rolling

Pan Lifang¹, Zhao Kaidong², Wang Shaohua³, Qin Chen¹, Jiao Haoyu¹, Liu Cuirong¹, Liu Guangming¹

¹ College of Materials Science and Engineering, Taiyuan University of Science and Technology, Taiyuan 030024, China; ² Shanxi Jianghuai Heavy Industry Co., Ltd, Jincheng 048026, China; ³ Taiyuan Jinxi Chunlei Copper Co., Ltd, Taiyuan 030008, China

Abstract: A mathematic model based on influence function method was established and the plan view pattern evolution rules of plates during angular rolling were studied by simulation and experimental methods. Results show that the difference in the elongation between the area near the angular point and other parts of the plate increases with the increase in the rotation angle of the first pass, which is the main reason why the length-width angle shows a downward trend with the increase in the rotation angle of the first pass. The length-width angle shows an upward trend with the increase in the rotation angle of the second pass, which can be attributed to the fact that the difference in the elongation between the area near the angular point (obtuse angle) and other parts of the plate increases with the increase in the rotation angle of the second pass. ε_w (the deformation in the width direction) increases with the increase in the rotation angle of the first or second pass, which is the primary reason why the width spread increases with the increase in the rotation angle of the first or second pass. Considering the same absolute reduction amount of the two passes, when the rotation angle of the second pass is two times the rotation angle of the first pass, the plates can return to almost rectangular. The predicted length-width angle and width spread values are in good agreement with the experimental ones, indicating that the established computational model based on influence function method can accurately estimate the length-width angle and width spread.

Key words: angular rolling; plan view pattern; influence function method; metal plate

In recent years, with the increasing market demand of the metal plates and strips with small batch and multiple specifications, the new requirements for flexible production of metal plates and strips have been put forward. At present, cross rolling spreading process is commonly used for the production of metal plates and strips. However, the per-pass reduction of cross rolling will be constrained when the width spread is too small and the cross rolling spreading process cannot be used to produce metal plates and strips when the workpiece is longer than the roll body. Therefore, the conventional rolling process is difficult to meet the growing demand for the metal plates and strips with non-standard specifications. The use of angular rolling contributes to the improvement in bite condition and rolling reduction and the decrease in the impact on the equipment during bite stage, and

it can also reduce the edge cracking of the plate and improve the internal microstructure. Moreover, with the use of angular rolling, the flexible spread rolling with small width spread ratios can be achieved, which is conducive to the reduction in the investment of continuous casting crystallizers and the realization of the production of the metal plates and strips with non-standard specifications. As a consequence, angular rolling process has received widespread attention in recent years as a flexible production technology^[1]. However, the study on angular rolling process is limited. Considering the widespread application of metal plates and strips and the numerous advantages of the angular rolling process, the research on the angular rolling process of metal plates and strips is absolutely essential.

At present, finite element method has become the most

Received date: May 17, 2023

Foundation item: Fund Program for the Scientific Activities of Selected Returned Overseas Professionals in Shanxi Province (20210046); (jiě bāng guà shuài) "Open Competition" Project: Preparation Technology and Product Development of Key New Materials for 5G Communication

Corresponding author: Liu Guangming, Professor, College of Materials Science and Engineering, Taiyuan University of Science and Technology, Taiyuan 030024, P. R. China, Tel: 0086-351-2776763, E-mail: 2011030@tyust.edu.cn

Copyright © 2023, Northwest Institute for Nonferrous Metal Research. Published by Science Press. All rights reserved.

popular method for studying the elastic deformation of rolling systems. Nevertheless, due to the long calculation time, this method applies only to offline calculation. Compared with finite element method, influence function method exhibits a higher accuracy and it requires a shorter calculation time, hence influence function method can be applied in the actual production process^[2]. Influence function method was proposed by Shohet et al in 1968^[3]. Since then, numerous studies on the use of influence function method have been carried out. Liu et al^[4] analyzed the stress of flatness measuring roll and established a deflection model for the flatness measuring roll using influence function method. Jiang et al^[5-6] simulated the cold rolling of thin strips and explored the influence of strip width on surface roughness through the use of the developed influence function method. Chai et al^[7] introduced the tilt variables of rolls and built an asymmetric deflection model based on influence function method. Chen et al^[8] established the online model of the elastic deformation of the roll using influence function method. Bu et al^[9] constructed a multi-objective function for the rolling production of thin gauge strips in tandem cold rolling mills based on influence function method. Ma et al^[10] calculated the screw-down load deviation affected by the additional moment employing influence function method. Liu et al^[11] established a deformation analysis model of top roll system and strips based on influence function method. Yu et al^[12] established the elastic deformation model of double cantilever beam roll system. Xie et al^[13] predicted roll deformation precisely and efficiently for the strip shape control of a six-high rolling mill. Hao et al^[2] established a mathematical model based on influence function method to accurately obtain the thickness distribution in the angular rolling process and to predict the rolling force. What needs to be pointed out is that the influence function method was used to calculate one section in the rolling process in most of the previous works. Nevertheless, in the angular rolling process, the volume and location of the metal in the deformation zone change with the increase in rolling time, which means that the shape of the roll gap also changes with rolling time. Therefore, in order to determine the width and position of the workpiece, a continuous computational model is needed.

In the present work, a mathematic model for the determination of the width and position of the workpiece was established based on influence function method. The plan view pattern evolution rules of plates during angular rolling were investigated by simulation and experimental methods.

1 Materials and Methods

1.1 Main mathematic model

1.1.1 Computational model based on influence function method

The work roll and plate are both divided into 60 pieces in the rolling direction, and the element division and numbering rules are shown in Fig.1. The distributed load applied to each element is represented by concentrated force. Moreover, the

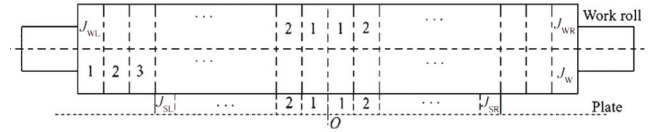


Fig.1 Schematic diagram of element division and numbering rules of work roll and plate

compatible deformation between two-roll mill and plate is calculated based on influence function method, during which two force-deformation relation equations and one compatibility equation of deformation are used, and the three equations can be written for matrix and vector forms as shown below.

(1) Elastic bending deformation equation of the work roll

$$Y_W = G_W P \tag{1}$$

where Y_W is work roll bending vector ($Y_W = [y_w(1) \cdots y_w(J_w)]^T$, y_w is the bending deflection of the roll); P is rolling force vector ($P = [p_L(J_{SL}) \cdots p_L(1) \quad p_R(1) \cdots p_R(J_{SR})]^T$, p is unit rolling force); G_W is the bending deformation influence function of the roll, which can be written in the following matrix form:

$$G_W = \begin{bmatrix} g_w(1, 1) & \cdots & g_w(1, J_w) \\ \vdots & \ddots & \vdots \\ g_w(J_w, 1) & \cdots & g_w(J_w, J_w) \end{bmatrix} \tag{2}$$

(2) Elastic flattening deformation equation of the work roll caused by rolling force:

$$Y_{WS} = G_{WS} P \tag{3}$$

where $Y_{WS} = [y_{WSL}(J_{SL}) \cdots y_{WSL}(1) \quad y_{WSR}(1) \cdots y_{WSR}(J_{SR})]^T$, y_{WS} is the flattening amount between the workpiece and roll; G_{WS} is the flattening deformation influence function of the roll caused by rolling force, which can be written in the following matrix form:

$$G_{WS} = \begin{bmatrix} g_{ws}(1, J_{WL} - J_{SL} + 1) & \cdots & g_{ws}(1, J_{WL} + J_{SL}) \\ \vdots & \ddots & \vdots \\ g_{ws}(J_w, J_{WL} - J_{SL} + 1) & \cdots & g_{ws}(J_w, J_{WL} + J_{SR}) \end{bmatrix} \tag{4}$$

(3) Compatibility equation of deformation between roll and workpiece

$$H = H_0 + Y_{WS} - Y_{WS0} - Y_W \tag{5}$$

where H is the thickness distribution vector of the workpiece above the symmetric line of top and bottom roll system ($H = [h_L(J_{SL}) \cdots h_L(1) \quad h_R(1) \cdots h_R(J_{SR})]^T$); H_0 is constant vector ($H_0 = [h(0) \cdots h(0)]^T$, $h(0)$ is half of the height of the workpiece at the center point of the workpiece); Y_{WS0} is constant vector ($Y_{WS0} = [y_{WS0}(0) \cdots y_{WS0}(0)]^T$, y_{WS0} is the flattening amount of the roll at the center of the workpiece).

1.1.2 Determination method of the width and position of the workpiece

Fig.2 shows the rotation position and segmentation of the workpiece. The diagonal intersection of the workpiece is set as origin of coordinates, the rolling centerline is set as y-axis, and the direction perpendicular to the rolling centerline is set

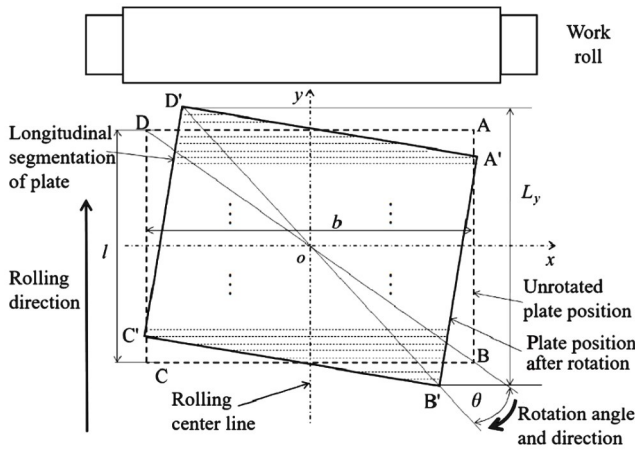


Fig.2 Schematic diagram of rotation position and segmentation of the workpiece

as x -axis. According to the rectangular coordinate system, the coordinates of the four vertexes of the workpiece before rotation can be obtained, which is shown below:

$$A\left(\frac{b}{2}, \frac{l}{2}\right); B\left(\frac{b}{2}, -\frac{l}{2}\right); C\left(-\frac{b}{2}, -\frac{l}{2}\right); D\left(-\frac{b}{2}, \frac{l}{2}\right)$$

where l is the length of the workpiece (mm), b is the width of the workpiece (mm). After clockwise rotation (the rotation angle is θ), the workpiece is in the initial position of the first-pass rolling and the coordinates of the four vertexes of the workpiece can be obtained as follows:

$$A'\left(\frac{b}{2} \cos \theta + \frac{l}{2} \sin \theta, -\frac{b}{2} \sin \theta + \frac{l}{2} \cos \theta\right)$$

$$W_{L,i} = \begin{cases} \left[\frac{1}{2}(b \sin \theta + l \cos \theta) - L_{y,i}\right](\tan \theta + \cot \theta), & \frac{l}{2}(\cos \theta + \sin \theta \tan \theta) \leq L_{y,i} < \frac{b}{2} \cos \theta + \frac{l}{2} \sin \theta \\ \frac{b}{2} \sin \theta \tan \theta + \frac{b}{2} \cos \theta - L_{y,i} \tan \theta, & 0 < L_{y,i} < \frac{l}{2}(\cos \theta + \sin \theta \tan \theta) \end{cases} \quad (9)$$

$$W_{R,i} = \begin{cases} 0, & \frac{l}{2}(\cos \theta + \sin \theta \tan \theta) < L_{y,i} < \frac{b}{2} \cos \theta + \frac{l}{2} \sin \theta \\ \left[\frac{l}{2}(\cos \theta + \sin \theta \tan \theta) - L_{y,i}\right] \cot \theta, & -\frac{b}{2} \sin \theta + \frac{l}{2} \cos \theta < L_{y,i} < \frac{l}{2}(\cos \theta + \sin \theta \tan \theta) \\ \frac{b}{2} \sin \theta \tan \theta + \frac{b}{2} \cos \theta + L_{y,i} \tan \theta, & 0 < L_{y,i} < -\frac{b}{2} \sin \theta + \frac{l}{2} \cos \theta \end{cases} \quad (10)$$

What needs to be pointed out is that after rotation, the workpiece is inversely symmetrical along the x -axis, so $W_{L,i}$ and $W_{R,i}$ corresponding to the pieces below the x -axis can also be computed in the same way.

1.1.3 Materials and angular rolling schedules used in the model analysis

The materials used in the present work were 5052 aluminum alloy plates with 10 mm in thickness, and the detailed material parameters and angular rolling schedules are shown in Table 1 and Table 2.

1.2 Experiment

The materials used in the experimental research were the same as the simulation ones. The experiment was carried out at room temperature using a two-high rolling mill with the

$$B\left(\frac{b}{2} \cos \theta - \frac{l}{2} \sin \theta, -\frac{b}{2} \sin \theta - \frac{l}{2} \cos \theta\right)$$

$$C\left(-\frac{b}{2} \cos \theta - \frac{l}{2} \sin \theta, \frac{b}{2} \sin \theta - \frac{l}{2} \cos \theta\right)$$

$$D'\left(-\frac{b}{2} \cos \theta + \frac{l}{2} \sin \theta, \frac{b}{2} \sin \theta + \frac{l}{2} \cos \theta\right)$$

The total length (L_y) of the workpiece along the rolling direction after rotation can be calculated by the following expression:

$$L_y = b \sin \theta + l \cos \theta \quad (6)$$

In addition, the workpiece after rotation is divided into $2n$ pieces in the rolling direction as shown in Fig.2. And when the deformation of each piece is calculated, the overall deformation of the workpiece can be obtained by the superposition of the deformation of each piece in the rolling and transverse directions.

The ordinate at the center line of each piece can be computed by the following equation:

$$L_{y,i} = \frac{(n - i + 1/2)}{2n} (b \sin \theta + l \cos \theta) \quad (7)$$

where i is the serial number of the pieces, $i=1-2n$. After rotation, the width of each piece in the rolling direction is different and the pieces are no longer symmetrical along the rolling center line. Therefore, the width of each piece can be calculated by the following equation:

$$W_i = W_{L,i} + W_{R,i} \quad (8)$$

where W_i is the total width of each piece (mm), $W_{L,i}$ is the width of each piece in the left side (mm), $W_{R,i}$ is the width of each piece in the right side (mm). $W_{L,i}$ and $W_{R,i}$ corresponding to the pieces above the x -axis can be computed by the following equations:

$$\frac{l}{2}(\cos \theta + \sin \theta \tan \theta) \leq L_{y,i} < \frac{b}{2} \cos \theta + \frac{l}{2} \sin \theta \quad (9)$$

$$0 < L_{y,i} < \frac{l}{2}(\cos \theta + \sin \theta \tan \theta)$$

$$\frac{l}{2}(\cos \theta + \sin \theta \tan \theta) < L_{y,i} < \frac{b}{2} \cos \theta + \frac{l}{2} \sin \theta$$

$$-\frac{b}{2} \sin \theta + \frac{l}{2} \cos \theta < L_{y,i} < \frac{l}{2}(\cos \theta + \sin \theta \tan \theta) \quad (10)$$

work roll length of 350 mm and the work roll diameter of 320 mm. The rolling speed was set as 200 mm·s⁻¹ and the reduction rates of the first and the second passes were set as 20% and 25%, respectively considering the same absolute reduction amount of the two passes, which were the same as the simulation ones. 0°, 10° and 40° were chosen as rolled plate rotation angles of the first pass; 0° (the rolled plate rotation angle of the first pass is 0°), 20° (the rolled plate

Table 1 Dimension and performance parameters of the aluminum alloy plates used in the present work

Length/ mm	Width/ mm	Thickness/ mm	Density/ g·cm ⁻³	Poisson's ratio
100	130	10	2.92	0.3

Table 2 Angular rolling schedules used in the present work

Parameter	Value
Work roll length/mm	350
Work roll diameter/mm	320
Rolling speed/mm·s ⁻¹	200
Rolling temperature/°C	25
Reduction rate of the first pass/%	20
Rolled plate rotation angles of the first pass	0°–40° (in steps of 10°)
Reduction rate of the second pass/%	25
Rolled plate rotation angles of the second pass	10°–50° (in steps of 10°, the rolled plate rotation angle of the first pass is 10°) 60°–100° (in steps of 10°, the rolled plate rotation angle of the first pass is 40°)

rotation angle of the first pass is 10°) and 80° (the rolled plate rotation angle of the first pass is 40°) were chosen as rolled plate rotation angles of the second pass.

2 Results and Discussion

2.1 Effect of rotation angle of the first pass on length-width angle and width spread

Fig. 3 presents the predicted plate shapes and the corresponding length-width angles (acute angles) and width spread. It can be seen that with the increase in the rotation angle of the first pass, the length-width angle shows a downward trend and the minimum value is 78.27°. Nevertheless, with the increase in the rotation angle of the first pass, the width spread exhibits an upward trend and it can reach 11.16 mm. Note that the “long-width angle” refers to the sharp angle between the long

edge and the short edge of the plate, and the “width spread” is measured by the distance between the two vertical edges.

Fig.4 displays the experimental plate shape. As can be seen, when the rotation angle is 0°, the length-width angle is 89.8° and the width spread is 1.7 mm. When the rotation angle is 10°, the length-width angle is 86° and the width spread is 2.1 mm. When the rotation angle increases to 40°, the length-width angle is 78° and the width spread can be 10.3 mm. In addition, the length-width angle decreases with the increase in rotation angle while the width spread demonstrates an opposite trend. Besides, average absolute relative error (AARE) is used to quantitatively analyze the error between the predicted results and the experimental ones. The smaller the AARE calculation result, the smaller the deviation between the predicted results and the experimental ones, and the stronger the predictive ability of the model. The calculation formula of AARE is:

$$AARE = \frac{1}{N} \sum_{i=1}^N \left| \frac{E_i - P_i}{E_i} \right| \times 100\% \tag{11}$$

where E is the experimental value, P is the predicted value, and N is the number of data.

After calculation, the AARE of length-width angle is 0.045%, and the AARE of width spread is 13.25%. From the above results, it is clear that the predicted length-width angle and width spread values are in good agreement with the experimental ones. It is indicated that the established computational model based on influence function method can give an accurate estimate for the length-width angle and width spread. Compared with finite element method^[2], influence function method exhibits a higher accuracy and requires a shorter calculation time.

In order to describe the metal flow rules during the first-pass angular rolling (natural width spread is disregarded), a schematic diagram has been drawn, as shown in Fig.5. As can be seen, when the rotation angle is θ_1 , the upper-right corner of the plate enters the deformation zone first, and with the increase in the horizontal distance to the angular point, the length of the plate along the rolling direction exhibits a decreasing trend ($l_0 > l_2 > l_1$ or $l_0 > l_3 > l_4$, only the upper half of the plate has been taken into account since the plate is inversely symmetrical along the horizontal center line of the plate), which means that the elongation of the upper-right corner of

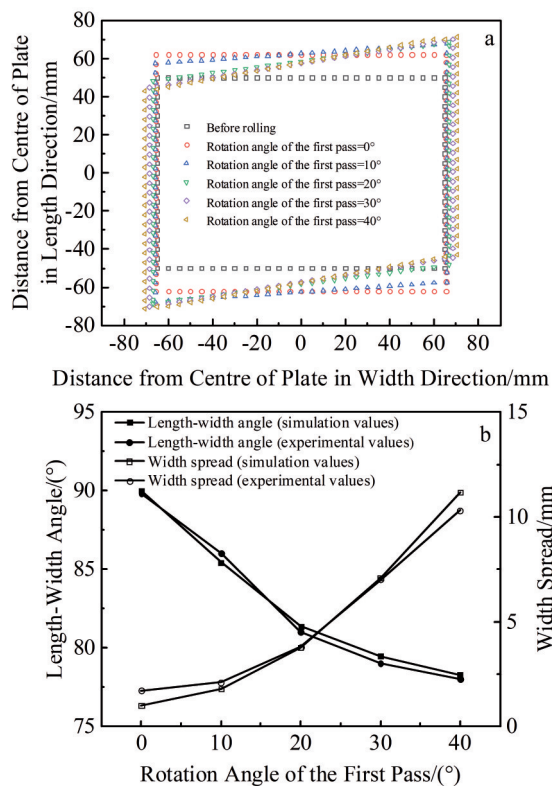


Fig.3 Predicted plate shapes (a) and the corresponding length-width angles and width spread (b)

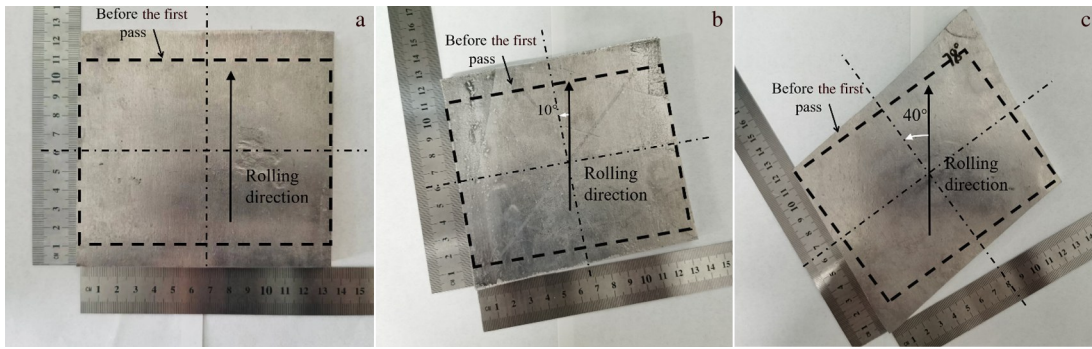


Fig.4 Experimental plate shapes with different rotation angles: (a) 0°, (b) 10°, and (c) 40°

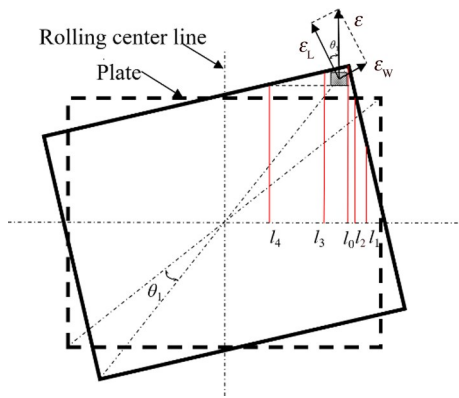


Fig.5 Schematic diagram of the metal flow during the first pass angular rolling

the plate will be larger than that of other parts of the plate due to the fact that at a given reduction rate, the longer the plate along the rolling direction, the larger the elongation will be. Owing to the above inhomogeneous deformation, the upper-right corner (length-width angle) will change from right angle (before rolling) to acute angle (after rolling). What needs to be pointed out is that with the increase in rotation angle, l_0 will be longer and the difference in the length of the plate along the rolling direction between the area near the angular point and other parts of the plate will increase, and consequently the difference in the elongation between the area near the angular point and other parts of the plate will also increase, which is the main reason why the length-width angle shows a downward trend with the increase in rotation angle. In addition, during first-pass angular rolling, there is an angle (θ_1) between the metal flow direction and the length direction of the plate, and thus the total deformation (ϵ) can be resolved into a deformation in the length direction (ϵ_L) and a deformation in the width direction (ϵ_w). The existence of ϵ_w can lead to an increase in the width of the plate and ϵ_w will increase with the increase in rotation angle. Therefore, the width spread demonstrates an upward trend with the increase in rotation angle.

2.2 Effect of rotation angle of the second pass on length-width angle and width spread

Fig. 6 displays the predicted plate shapes and the corresponding length-width angles (acute angles) and width spread

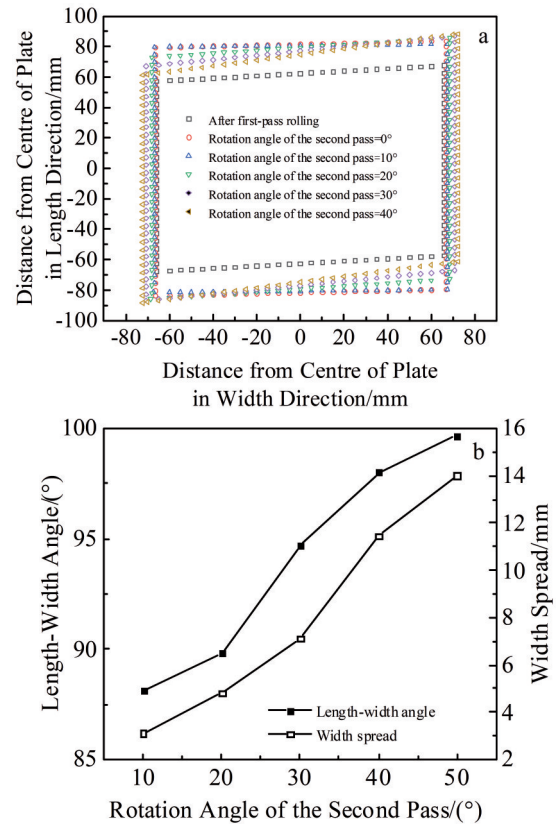


Fig.6 Predicted plate shapes (a) and the corresponding length-width angles and width spread (b) when the rotation angle of the first pass is 10°

(the rotation angle of the first pass is 10°). As can be seen, both the length-width angle and width spread show an upward trend with the increase in the rotation angle of the second pass. The maximum length-width angle is close to 100°, and the maximum width spread can reach 14.4 mm. In addition, it should be pointed out that when the rotation angle is 20°, the length-width angle is 89.8° (the plate is almost rectangular), which means that angle combination of 10° (the rotation angle of the first pass) +20° (the rotation angle of the second pass) can be used to produce rectangular workpiece.

Fig. 7 presents the predicted plate shapes and the corresponding length-width angles and width spread (the rotation

angle of the first pass is 40°). It can be clearly seen that the width spread increases with the increase in the rotation angle of the second pass and the maximum value is 33 mm. And with the increase in the rotation angle of the second pass, the length-width angle increases first and then decreases, and the maximum value is 89.65° . At this point, the plate is almost rectangular, which means that angle combination of 40° (the rotation angle of the first pass) + 80° (the rotation angle of the second pass) can also be used to produce rectangular workpiece and it is reasonable to infer that when the rotation angle of the second pass is two times larger than the rotation angle of the first pass, the workpiece will return to almost rectangular. To verify this hypothesis, more angle combinations are chosen in the simulation study and the results are shown in Fig. 8. As can be seen, the length-width angles are close to 90° regardless of the angle combinations, which signifies that the above speculation is correct. Moreover, it should be noted that the width spread increases with the increase in rotation angle. Therefore, in practical production, different angle combinations can be selected to produce the plates with different widths.

Fig. 9 shows the experimental plate shape when different angle combinations are used. As can be seen, when $0^\circ + 0^\circ$ angle combination is used, the length-width angle is 89.4° and

the width spread is 3.8 mm. When $10^\circ + 20^\circ$ angle combination is used, the length-width angle is 89.4° and the width spread is 5.2 mm. And when $40^\circ + 80^\circ$ angle combination is used, the length-width angle is 89.2° and the width spread is 29.3 mm. Moreover, the calculated AARE of width spread is 3.63%.

From the results in this section, it is clear that the predicted length-width angle and width spread values are in good agreement with the experimental ones, which proves once again that the established computational model based on influence function method has a high accuracy. In order to describe the metal flow rules during the second pass angular rolling (natural width spread is disregarded), a schematic diagram is drawn as shown in Fig. 10. As can be seen, when the rotation angle is θ_2 , the upper-left corner (obtuse angle) of the plate enters the deformation zone first. It can be seen from the analysis in Section 2.1 that the elongation of the upper-left corner of the plate will be larger than that of other parts of the plate, leading to an decrease in the degree of the obtuse angle, and as a result, the length-width angle (acute angle) increases. Since the difference in the elongation between the area near the angular point and other parts of the plate increases with the increase in the rotation angle of the second pass, the length-width angle (acute angle) will show an upward trend with the increase in the rotation angle of the second pass. It

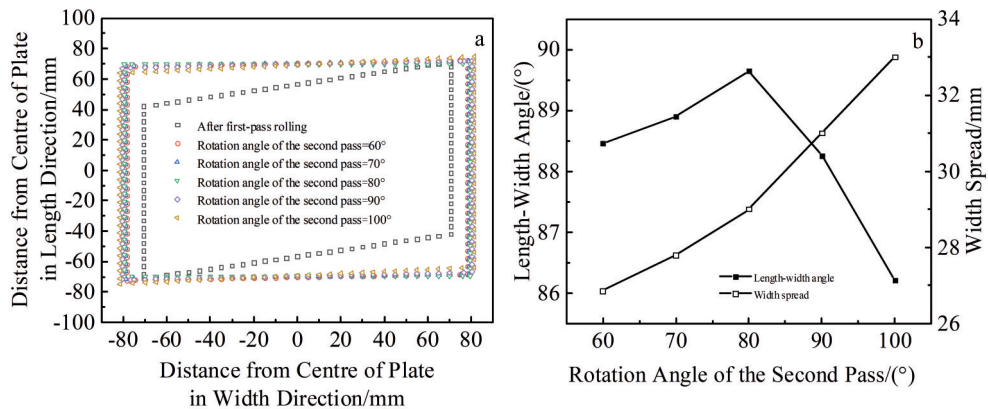


Fig.7 Predicted plate shapes (a) and the corresponding length-width angles and width spread (b) when the rotation angle of the first pass is 40°

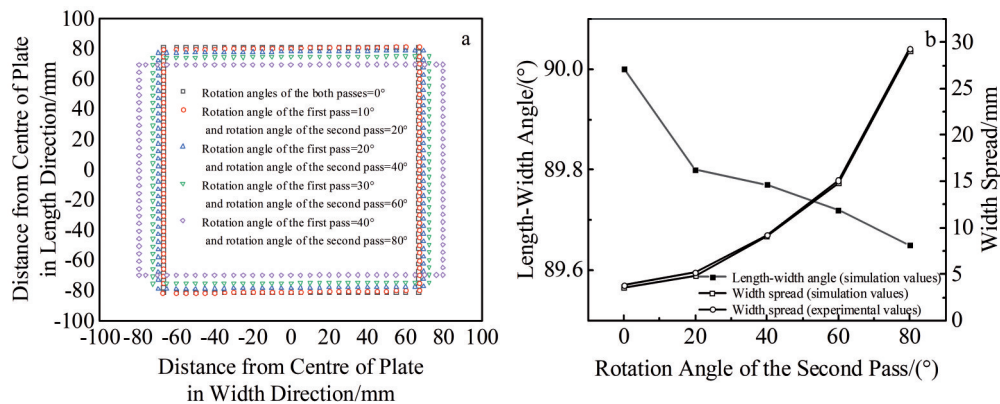


Fig.8 Predicted plate shapes (a) and the corresponding length-width angles and width spread (b) when the rotation angle of the second pass is two times larger than the rotation angle of the first pass

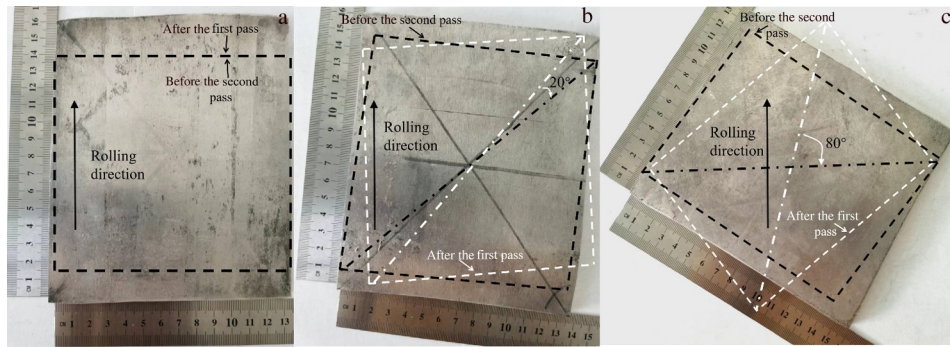


Fig.9 Experimental plate shapes under different angle combinations: (a) $0^{\circ}+0^{\circ}$, (b) $10^{\circ}+20^{\circ}$, and (c) $40^{\circ}+80^{\circ}$

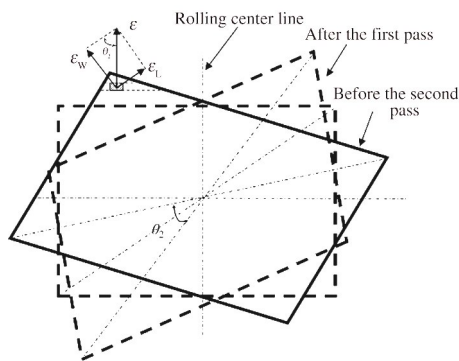


Fig.10 Schematic diagram of the metal flow during the second pass angular rolling

should be pointed out that when the rotation angle of the first pass is 40° and the rotation angle of the second pass is over 80° , the length-width angle exhibits a decreasing trend with the increase in the rotation angle of the second pass, which can be ascribed to the fact that with the increase in the rotation angle of the second pass (over 80°), the metal flow in the rolling direction decreases. In addition, during second-pass angular rolling, the existence of ε_w can lead to the increase in the width of the plate and ε_w will increase with the increase in the rotation angle of the second pass. Therefore, the width spread exhibits an upward trend with the increase in the rotation angle of the second pass regardless of the rotation angle of the first pass.

3 Conclusions

1) The length-width angle decreases with the increase in the rotation angle of the first pass, which can be attributed to the fact that the difference in the elongation between the area near the angular point and other parts of the plate increases with the increase in the rotation angle of the first pass.

2) The length-width angle exhibits an increasing trend with the increase in the rotation angle of the second pass, which can be ascribed to the fact that the difference in the elongation between the area near the angular point (obtuse angle) and other parts of the plate increases with the increase in the rotation angle of the second pass.

3) The width spread increases with the increase in the

rotation angle of the first or the second pass and the main reason is that ε_w (the deformation in the width direction) shows an upward trend with the increase in the rotation angle of the first or the second pass.

4) Considering the same absolute reduction amount of the two passes, when the rotation angle of the second pass is two times larger than the rotation angle of the first pass, the plates can return to almost rectangular.

5) The predicted length-width angle and width spread values are in good agreement with the experimental ones, indicating that the established computational model based on influence function method has a high accuracy.

References

- 1 Lou H F, Huang H, Liang X P et al. *Strategic Study of Chinese Academy of Engineering*[J], 2020, 22(5): 68
- 2 Hao P J, He A R, Sun W Q. *Mechanics & Industry*[J], 2018, 19(3): 1
- 3 Shohet K N, Townsend N A. *Journal of the Iron and Steel International*[J], 1968, 206(11): 1088
- 4 Liu J W, Zhang D H, Wang J S et al. *Journal of Iron and Steel Research International*[J], 2010, 17(12): 35
- 5 Jiang Z Y, Zhu H T, Tieu A K. *International Journal of Mechanical Sciences*[J], 2006, 48(7): 697
- 6 Jiang Z Y, Wei D, Tieu A K. *Journal of Materials Processing Technology*[J], 2009, 209(9): 4584
- 7 Chai X J, Li H B, Zhang J et al. *Atlantis Press*[J], 2015: 1063
- 8 Chen S, Peng L, Wang L et al. *Journal of Central South University (Science and Technology)*[J], 2017, 48(6): 1432
- 9 Bu H N, Yan Z W, Zhang D H et al. *Scientia Iranica*[J], 2016, 23(6): 2663
- 10 Ma X B, Liu H M, Sun J L et al. *Engineering Failure Analysis*[J], 2017, 79: 913
- 11 Liu G M, Li Y G, Huang Q X et al. *Mathematical Problems in Engineering*[J], 2018, 2018: 7 527 402
- 12 Yu H, Li W, Huang Z M et al. *Rare Metal Materials and Engineering*[J], 2020, 49(7): 2220
- 13 Xie L, He A R, Liu C. *Journal of Iron and Steel Research International*[J], 2018, 25(9): 901

板材角轧过程平面形状演变规律

潘丽芳¹, 赵凯东², 王少华³, 秦晨¹, 焦皓宇¹, 刘翠荣¹, 刘光明¹

(1. 太原科技大学 材料科学与工程学院, 山西 太原 030024)

(2. 山西江淮重工有限公司, 山西 晋城 048026)

(3. 太原市晋西春雷铜业有限公司, 山西 太原 030008)

摘要: 建立了基于影响函数法的数学模型, 利用仿真和实验方法研究了角轧制过程中板块的平面板形演化规律。结果表明, 随着第1道旋转角度的增加, 板材角部与其他部位的伸长率差异增大, 这是长宽夹角随第1道旋转角度增大而呈下降趋势的主要原因。随着第2道旋转角度的增加, 长宽角呈上升趋势, 这是由于板材角部(钝角)与他部位的伸长率差异随着第2道旋转角度的增加而增大。 ε_w (宽度方向上的变形) 随着第1道或第2道旋转角度的增加而增大, 这是宽展随第1道或第2道旋转角度增大的主要原因。考虑到2次轧制的压下量相同, 当第2道的旋转角度是第1道旋转角度的2倍时, 板材几乎可以恢复到矩形。预测的长宽夹角和宽展值与实验值吻合较好, 表明所建立的基于影响函数法的计算模型能够准确估计长宽夹角和宽展。

关键词: 角轧; 平面形状; 影响函数法; 金属板材

作者简介: 潘丽芳, 女, 1981年生, 博士生, 太原科技大学材料科学与工程学院, 山西 太原 030024, E-mail: 2013017@tyust.edu.cn